

## Titanium dioxide - activated carbon composite for photoelectrochemical degradation of phenol

L. H. Q. Anh <sup>a</sup> , Uyen P. N. Tran <sup>b</sup> , P. V. G. Nghi <sup>c</sup>, H. T. Le <sup>c</sup>,  
N. T. B. Khuyen <sup>d\*</sup>, T. D. Hai <sup>e\*</sup> 

a: Faculty of General Sciences, Ho Chi Minh city University of Natural Resources and Environment, Ho Chi Minh city 70000, Vietnam

b: Faculty of Engineering and Technology, Van Hien University, Ho Chi Minh city 70000, Vietnam

c: Faculty of Applied Science, Ton Duc Thang University, Ho Chi Minh city 70000, Vietnam

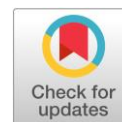
d: Office of R&D and External Relations, Ho Chi Minh city University of Natural Resources and Environment, Ho Chi Minh city 70000, Vietnam

e: Faculty of Environment, Ho Chi Minh city University of Natural Resources and Environment, Ho Chi Minh city 70000, Vietnam

\* Corresponding author: [ntbkhuyen@hcmunre.edu.vn](mailto:ntbkhuyen@hcmunre.edu.vn), [tdhai@hcmunre.edu.vn](mailto:tdhai@hcmunre.edu.vn)

This paper belongs to a Regular Issue.

© 2022, the Authors. This article is published in open access under the terms and conditions of the Creative Commons Attribution (CC BY) license (<http://creativecommons.org/licenses/by/4.0/>).



### Abstract

In this study, titanium dioxide (TiO<sub>2</sub>) and titanium dioxide – activated carbon composite (TiO<sub>2</sub>-AC) were prepared by sol-gel method for photoelectrochemical (PEC) applications. Characterization of the materials was performed by scanning electron microscope, energy dispersive X-ray analysis, Fourier transform infrared spectroscopy, X-ray diffraction, and diffuse reflectance spectroscopy. The results show that TiO<sub>2</sub> was successfully loaded on activated carbon (AC), producing TiO<sub>2</sub>-AC with 2.61 eV of bandgap energy, lower than that of TiO<sub>2</sub> (3.15 eV). Photoanodes based on TiO<sub>2</sub> and TiO<sub>2</sub>-AC were fabricated and applied to PEC experiments for phenol degradation. In comparison with the TiO<sub>2</sub> photoanode, the TiO<sub>2</sub>-AC one exhibited superior photocatalytic activity, which was indicated by a high current density and effective phenol removal. A mechanism of phenol PEC degradation on the TiO<sub>2</sub>-AC photoanode was proposed, which includes interaction between protonated phenol and active sites bearing oxygen on the photoanode surface. A kinetic model according to this mechanism was also established and fitted to experimental findings, resulting in rate constants of elementary reactions.

### Keywords

Photoelectrochemical  
Titanium dioxide  
Phenol degradation  
Photocatalyst  
Kinetic model

Received: 17.09.22

Revised: 15.10.22

Accepted: 16.10.22

Available online: 25.10.22

## 1. Introduction

Phenol and phenolic compounds are commonly used in pharmaceuticals, insecticides, cosmetics, and other industrial substances [1]. Phenol is known as a hazardous pollutant due to its toxicity and high stability for a long period of time in the environment [2, 3]. Phenol exposure may cause acute and/or chronic diseases on the skin, eye, respiratory and nervous systems [4, 5]. There are some techniques for phenol removal from wastewater, as summarized in [6]. Among advanced oxidation processes, photocatalysis is described as an effective choice for phenol degradation. Based on TiO<sub>2</sub> photocatalyst synthesized by the sol-gel method, phenol degradation was attained at 58.8% after 240 minutes of UV illumination [7]. In the presence of carbon, photogenerated charge recombination of TiO<sub>2</sub> was

delayed [8], suggesting an improvement in phenol degradation. Synergy effect between TiO<sub>2</sub> and carbon-based materials was explored in the previous reports on multi-walled carbon nanotubes – TiO<sub>2</sub> [9], activated carbon – TiO<sub>2</sub> [10], graphene – TiO<sub>2</sub> [11], and carbon fiber – TiO<sub>2</sub> [12].

Difficult recovery and fast photoexcited electron-hole pairs recombination of catalysts are two considerable drawbacks of photocatalysis, which can be minimized with the photoelectrochemical (PEC) method [13, 14]. According to the PEC principle, a photocatalyst is coated onto a photoelectrode, to which a bias voltage is applied to improve photogenerated charge carrier separation, thus enhancing the activity of the photocatalyst [15, 16]. Therefore, the PEC method has attracted considerable interest in water splitting [17] as well as organic pollutants degradation [13]. Us-

ing a TiO<sub>2</sub>-based photoanode for the PEC experiment, phenol degradation achieved 73.76% after 120 minutes of UV illumination under 0.8 V of applied voltage [18]. By adding peroxymonosulfate into the PEC system, a photoelectrode based on Co<sub>3</sub>O<sub>4</sub>-loaded carbon fiber demonstrated 100% phenol degradation within 90 minutes under UV radiation at 1.5 V of applied voltage [19]. The contribution of carbon to PEC behavior of the C/TiO<sub>2</sub> composite was explored by Haro et al. [20]. It was found out that carbon promoted charge transfer reactions on C/TiO<sub>2</sub> photoelectrode surface through enhancement of charge carrier generation and separation. However, the application of C/TiO<sub>2</sub> in PEC degradation of organic compounds has not been reported in the literature.

In this study, TiO<sub>2</sub> and TiO<sub>2</sub>-activated carbon (TiO<sub>2</sub>-AC) composites were synthesized by a sol-gel method for PEC degradation of phenol. Effects of AC on PEC properties of the TiO<sub>2</sub>/AC photoanode for phenol were determined. Moreover, a mechanism of phenol PEC degradation was proposed, revealing a kinetic model describing the surface responses of the TiO<sub>2</sub>/AC photocatalyst.

## 2. Experiment

### 2.1. Materials, chemicals and apparatus

Pure titanium tetrachloride (TiCl<sub>4</sub>) (99.99%) was purchased from Shanghai Aladdin Bio-Chem Technology Co., Ltd (China). Commercial activated carbon (AC), ethanol (99%), phenol (>99%), and hexane (>96%) were obtained from Xilong Scientific Co., Ltd (China). Hydrochloric acid (HCl, 36.5% w/w), sodium hydroxide (NaOH, >99%) were bought from Merck (Germany). Liquid polyester resin was collected from En chuan Chemical Industries Co., Ltd (Taiwan). 1-Butyl-1-Methylpyrrolidinium hexafluorophosphate (BMIM FP6, 97.5%) was supplied by IndianMart. Tap water was used to prepare all solutions.

Characterization of materials was conducted with analytical methods such as scanning electron microscopy (SEM) and energy dispersive X-ray (EDX) using Prisma E SEM, X-ray diffraction (XRD) recording by D2 PHASER, diffuse reflectance spectra carried out by FL-1039 (HORIBA), Fourier-transform infrared spectroscopy (FT-IR) with Nicolet iS5, current – voltage (J-V) curve and electrochemical impedance spectroscopy (EIS) using MPG2 Biologic system.

### 2.2. Preparation of TiO<sub>2</sub>, TiO<sub>2</sub>-AC composite, and photoanodes

10 ml of TiCl<sub>4</sub> and 10 g of AC were added into an Erlenmeyer flask containing 200 ml of hexane under N<sub>2</sub> atmosphere in a glovebox. The Erlenmeyer flask was then covered and moved to an ultrasonic tank. The mixture was dispersed under 40 kHz of sonication for 15 minutes before adding 500 ml of distilled water. After 30 minutes of sonication, the solid phase was separated and washed with distilled water in a vacuum filtration system until the filtrate reached neutral pH. The obtained solid was thermally treated at 550 °C

for 30 minutes to produce the TiO<sub>2</sub>-AC photocatalytic composite.

To prepare the TiO<sub>2</sub> photocatalyst, the above procedure was applied without AC.

A coating mixture (consisting of 80% w/w of polyester, 19% w/w of ethanol, and 1% w/w of BMIM PF6) was deposited onto a SUS 304 stainless sheet (0.8 mm of thickness, 100×100 mm of dimension) as a photoanode substrate by the dip-coating method. Then, an abundant amount of photocatalyst was spread on the photoanode surface and pressed under 3 N/cm<sup>2</sup> of pressure to create contact between the photocatalyst and the photoanode substrate. The obtained photoanodes based on TiO<sub>2</sub> and TiO<sub>2</sub>-AC photocatalysts were stored at room temperature for one week before being utilized in the PEC system.

### 2.3. Photoelectrochemical measurements

A three-electrode cell was used for PEC measurements with a Pt grid as a counter electrode, an Ag/AgCl as a reference electrode, the photoanode as a working electrode, and a UV-C mercury lamp (9 W) vertically soaked in a solution. All PEC measurements were conducted under fluorescent light (400–600 lux of illumination) in a 10 mg/L of phenol solution, pH = 5 with UV and non-UV radiation. The J-V curves were recorded according to the linear sweep voltammetry technique in a potential range of 0 V to +1.5 V at a scan rate of 50 mV/s. The EIS characteristics were obtained over a frequency range of 10 mHz to 10 kHz with 10 mV amplitude.

### 2.4. Photoelectrochemical degradation of phenol

Bath experiments for PEC degradation of phenol under UV and non-UV illumination were performed in a stirred PEC reactor containing 1 liter of phenol solution. The Pt grid and photoanode were vertically dipped into phenol solution and connected to a controllable DC voltage source. Between the Pt grid and the photoanode, the UV-C lamp was also immersed in the solution. Phenol concentration was determined by the colorimetric method using HI 3864 phenol test kit with the instrumental error up to 0.1 mg·L<sup>-1</sup>. The efficiency of phenol removal was calculated by Equation (1).

$$\text{Phenol removal (\%)} = \left(1 - \frac{C_t}{C_o}\right) \times 100 \quad (1)$$

where C<sub>t</sub>, C<sub>o</sub> are the concentrations of phenol after contact time *t* and at the start (initial concentration) in mg·L<sup>-1</sup>, respectively.

## 3. Results and Discussion

### 3.1. Characterization of materials

The morphology of TiO<sub>2</sub>, AC and TiO<sub>2</sub>-AC can be observed in SEM images. As shown in Figure 1a, TiO<sub>2</sub> particles are irregular polygonal shapes that are less than 25 μm in size. Porous structure with cavities and pits of AC is disclosed in Figure 1b.

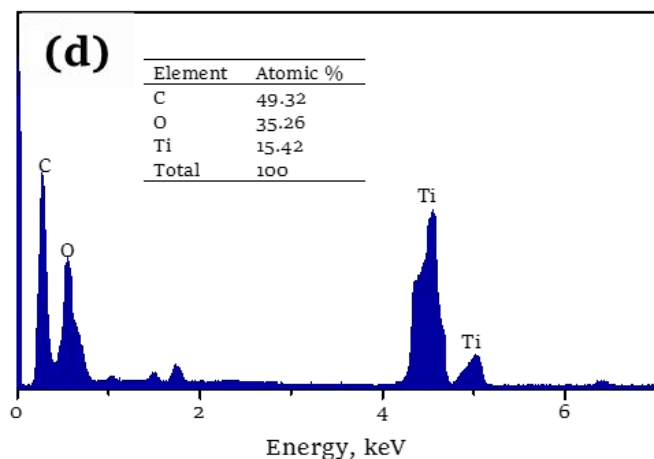
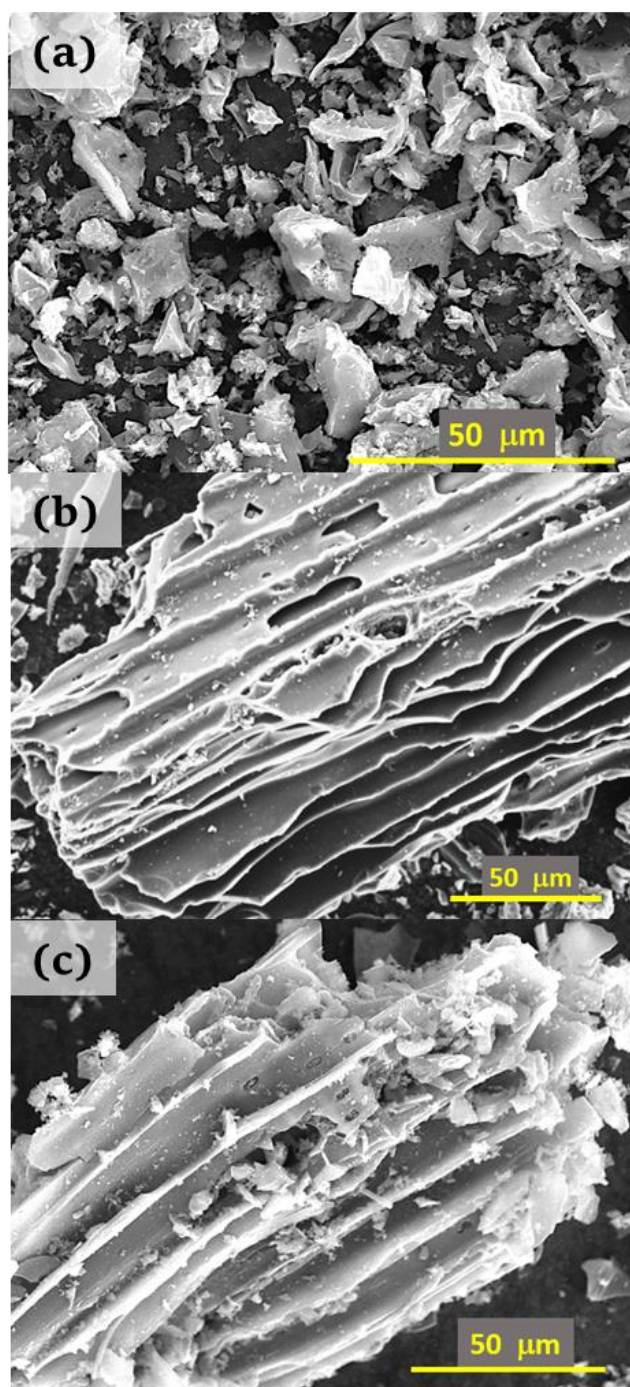


**Figure 1** SEM images of TiO<sub>2</sub> (a), AC (b), TiO<sub>2</sub>-AC (c), and EDX spectrum of TiO<sub>2</sub>-AC (d).

For TiO<sub>2</sub>-AC, a large number of TiO<sub>2</sub> particles was loaded on AC structure by filling into the pits instead of the surface of cavities, as shown in Figure 1c. Similar observation was also reported in a previous publication [21]. Located in pits, TiO<sub>2</sub> particles could avoid being washed out from AC in photoanode preparation and utilization. As expected, C, O, and Ti elements in TiO<sub>2</sub>-AC were indicated in the EDX results, as shown in Figure 1d.

Crystal phase characteristics of TiO<sub>2</sub>, AC, and TiO<sub>2</sub>-AC were explored with X-ray diffraction analysis as shown in Figure 2. The reflections from the (002) and (100) planes of aromatic rings of amorphous carbon structure caused the diffraction peaks at 26.2° and 43.5° [22]. For the XRD pattern of TiO<sub>2</sub>, peaks appearing at 27.7°, 36.1°, 41.2°, 54.2°, and 56.7° were indexed as (110), (101), (111), (211), and (220) planes of rutile phase, whereas the presence of anatase phase was identified by the peaks at 25.3° and 48.3°, according to (101) and (200) planes [23]. However, only characteristic peaks of rutile TiO<sub>2</sub> exist in TiO<sub>2</sub>-AC material, as shown in the XRD pattern of TiO<sub>2</sub>-AC. This may be due to the effect of carbon on anatase to rutile transformation of TiO<sub>2</sub> through the formation of oxygen vacancies, as mentioned in [24–26]. This is a disadvantage of our TiO<sub>2</sub>-AC because rutile TiO<sub>2</sub> exhibits lower photocatalytic activity than anatase TiO<sub>2</sub> [27].

Chemical bonds in TiO<sub>2</sub>, AC, and TiO<sub>2</sub>-AC were identified by FTIR analysis (Figure 3). As shown in the FTIR spectrum of TiO<sub>2</sub>, a strong absorption band at about 500 cm<sup>-1</sup> reflects the vibration of Ti–O bond, and a band at 1653 cm<sup>-1</sup> corresponds to O–H bending in absorbed water molecules [28]. Stretching vibrations of C–O and C=C bonds in AC structure were identified by bands at 1097 cm<sup>-1</sup> and 1554 cm<sup>-1</sup>, respectively [29]. A band appearing at 3469 cm<sup>-1</sup> is associated with the stretching vibration of O–H bond and free water [28]. It can be observed in the FTIR spectrum of TiO<sub>2</sub>-AC that characteristic bands of the bonds in TiO<sub>2</sub> and AC appeared again without a new band, indicating TiO<sub>2</sub> did not conjugate to AC in TiO<sub>2</sub>-AC by a chemical bond. A similar result could be found in [21, 30].

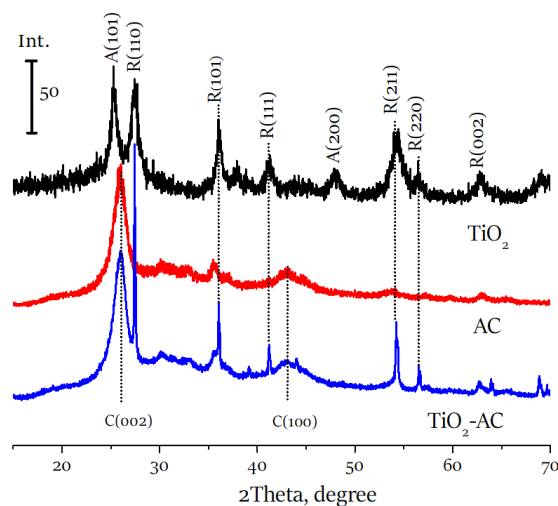


**Figure 2** XRD patterns of materials.

As presented in Figure 4a, UV-Vis diffuse reflectance spectra of  $\text{TiO}_2$  and  $\text{TiO}_2\text{-AC}$  shows the absorption edge of the  $\text{TiO}_2$  and  $\text{TiO}_2\text{-AC}$  at about 370 nm and 420 nm, respectively. It indicates the red-shift of the  $\text{TiO}_2\text{-AC}$  towards the visible region in comparison with  $\text{TiO}_2$ . Tauc plots, relationships of  $h\nu$  vs  $(\alpha h\nu)^{1/2}$  of materials, are illustrated in Figure 4b, revealing band gap energies of 3.15 eV and 2.61 eV for  $\text{TiO}_2$  and  $\text{TiO}_2\text{-AC}$ , respectively. Carbon not only promotes the  $4p \rightarrow 4s$  electronic transition at defect points in the titanium atoms [31], but also improves the electron transfer due to the high electronic conductivity of carbon, thereby resulting in the lower band gap energy of  $\text{TiO}_2\text{-AC}$  compared to  $\text{TiO}_2$ . This result indicates that  $\text{TiO}_2\text{-AC}$  can effectively separate electron-hole pairs in the visible region, which promotes photocatalytic activity under the solar illumination.

### 3.2. Characterization of photoanodes

A  $\text{TiO}_2\text{-AC}$  photoanode was selected for morphological analysis by the SEM technique. It can be observed in Figure 5a that  $\text{TiO}_2\text{-AC}$  particles in random shapes were widely spread on the photoanode surface generating a rough structure. The original morphology of  $\text{TiO}_2\text{-AC}$  (Figure 1c) exposed on the photoanode surface (as shown in Figure 5b) indicated that  $\text{TiO}_2\text{-AC}$  particles were not immersed completely in the coating mixture. It proves that photoactive sites in  $\text{TiO}_2\text{-AC}$  were disclosed on the photoanode surface, enabling photoexcitation of the  $\text{TiO}_2\text{-AC}$  photoanode in the photoelectrochemical system. The mean thickness of a coated layer on the photoanode was determined to be 136  $\mu\text{m}$ .

Photoelectrochemical properties of the  $\text{TiO}_2$  and  $\text{TiO}_2\text{-AC}$  photoanodes were examined using a three-electrode cell in phenol solution at pH = 5. Figure 6 demonstrates the current density of the  $\text{TiO}_2$  and  $\text{TiO}_2\text{-AC}$  photoanodes under non-UV and UV illumination applying linear sweep voltammetry. In the absence of UV (non-UV), photoanodes present low current density. Under UV radiation, photocurrent densities of photoanodes significantly increase. The  $\text{TiO}_2\text{-AC}$  photoanodes generated a current density of 283  $\mu\text{A}/\text{cm}^2$  (at 1.45 V vs. Ag/AgCl), which is approximately 2.2 times higher than that of the  $\text{TiO}_2$  photoanode. This result may be due to the decrease of  $\text{TiO}_2$  band gap in the presence of AC. Photocatalytic activity of a photoanode driving a reaction can be evaluated through an onset potential, which is a potential at the intersection point between J-V curve in non-UV radiation and the tangent line with a maximum slope of J-V curve in UV radiation [32, 33]. The onset potential of the  $\text{TiO}_2$  photoanode driving phenol oxidation ( $\sim 1.0$  V vs Ag/AgCl) is about 350 mV higher than that of the  $\text{TiO}_2\text{-AC}$  photoanode ( $\sim 0.66$  V vs Ag/AgCl), indicating heterojunction formation of  $\text{TiO}_2/\text{AC}$  in the  $\text{TiO}_2\text{-AC}$  material [34]. The low onset potential of the  $\text{TiO}_2\text{-AC}$  photoanode demonstrated an effective charge separation and transfer, manifesting a favorable application of the  $\text{TiO}_2\text{-AC}$  photoanode for PEC degradation of phenol.

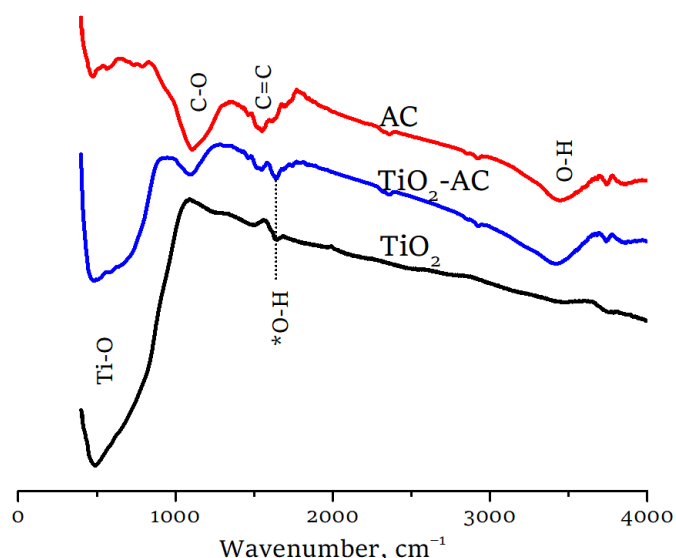


Figure 3 FTIR spectra of materials.

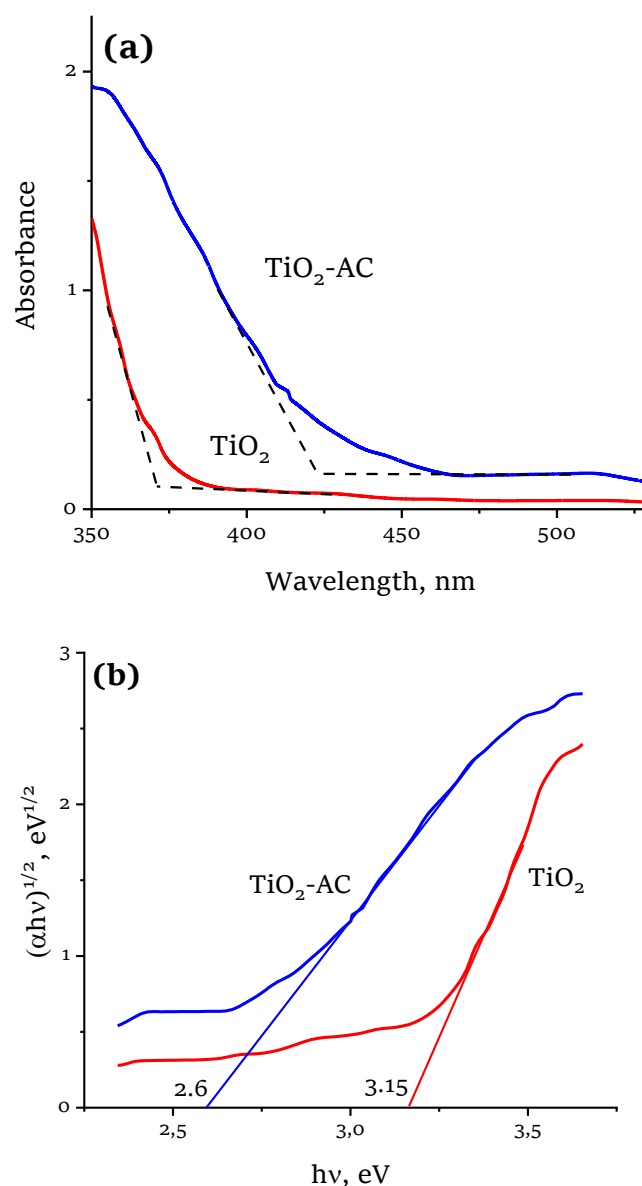


Figure 4 Curves of UV-Vis diffuse reflectance spectra (a) and Tauc plots of  $\text{TiO}_2$  and  $\text{TiO}_2\text{-AC}$  materials (b).

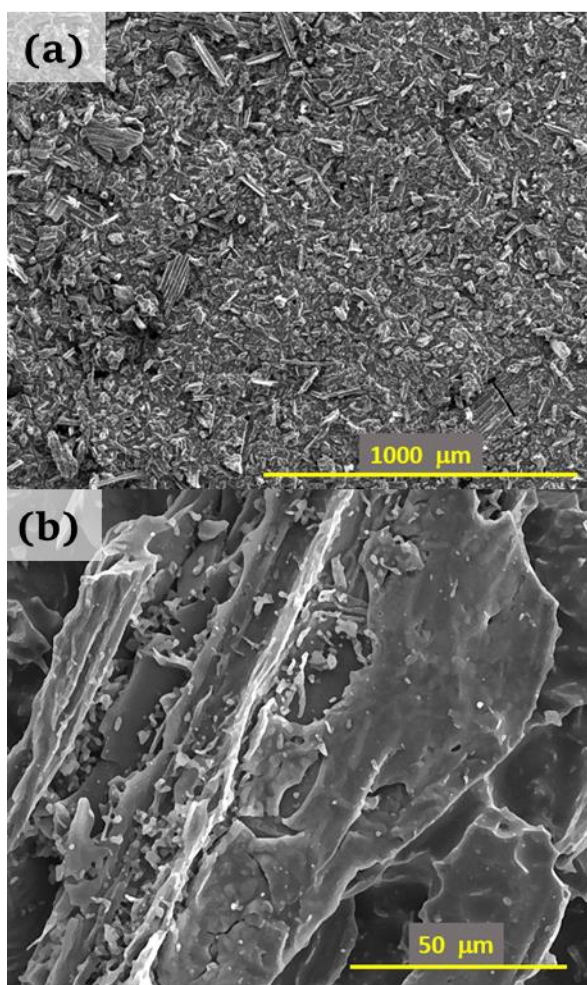


Figure 5 SEM images of TiO<sub>2</sub>-AC photoanode surface in 80x (a) and 1200x (b).

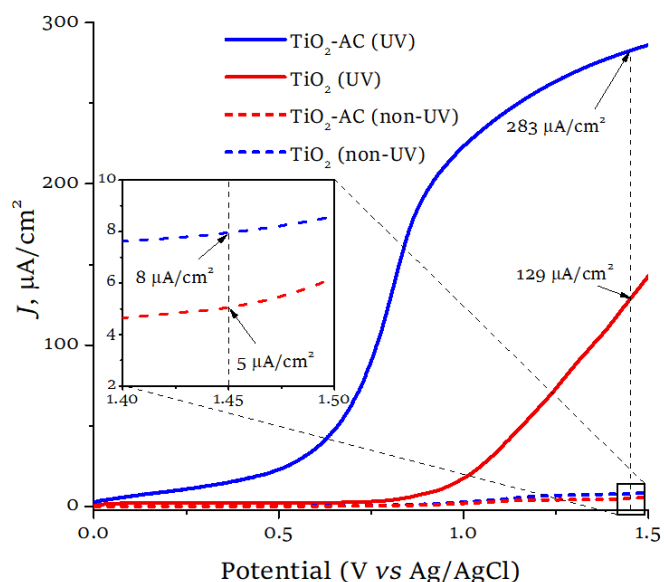


Figure 6 Current - voltage (*J*-*V*) curves of photoanodes in 10 mg/L of phenol solution (pH = 5).

Figure 7 presents Nyquist plots of TiO<sub>2</sub> and TiO<sub>2</sub>-AC photoanodes under UV and non-UV illumination. There is only one semicircle for each Nyquist plot, indicating that PEC process on the photoanodes for phenol was controlled by trap electron transfer [35]. Smaller diameter semicircle

demonstrates lower charge transfer resistance [36]. It can be observed clearly from Figure 7 that the semicircle in the Nyquist plot of the TiO<sub>2</sub> and TiO<sub>2</sub>-AC photoanodes under UV radiation is smaller than that under the non-UV excitation. This finding proves that the charge transfer of photoanodes was improved under UV illumination. The TiO<sub>2</sub>-AC photoanode exhibited a better charge transfer in comparison to TiO<sub>2</sub> one because Nyquist plots of the TiO<sub>2</sub>-AC photoanode show smaller semicircles in both UV and non-UV excitation. This result indicates that the presence of AC not only did not reduce the photocatalytic properties of TiO<sub>2</sub>, but also improved the electrical conductivity of TiO<sub>2</sub>-AC, advancing the applicability of the TiO<sub>2</sub>-AC photoanode in PEC process.

### 3.3. Photoelectrochemical degradation of phenol

Applied external voltage (*V*<sub>app</sub>) can improve PEC performance of TiO<sub>2</sub> by enhancing the generation and separation of charge carriers [37]. After 30 minutes of PEC treatment under different *V*<sub>app</sub> in the range of 0–0.7 V, phenol and COD removal at the TiO<sub>2</sub>-AC photoanode were recorded and shown in Figure 8a. Phenol and COD removal exhibit similar trends under *V*<sub>app</sub> variation. Phenol can be converted to organic intermediates during the photocatalysis process before it is completely oxidized to CO<sub>2</sub> [38]. If COD removal equates to phenol removal, the total removed phenol is oxidized to CO<sub>2</sub> without the formation of intermediates. As illustrated in Figure 8a, the ratio of phenol and COD removal decreases to approximately 1 with the increase of *V*<sub>app</sub>, corresponding to 15.50, 13.67, 7.45, 2.58, 1.04, and 1.04 for 0, 0.2, 0.4, 0.5, 0.6, and 0.7 V of *V*<sub>app</sub>, respectively. Dependences of phenol and COD removal as a function of *V*<sub>app</sub> present a break-like point at 0.4 V and an exhaustion-like point at 0.6 V (Figure 8a), which is close to the onset potential of the TiO<sub>2</sub>-AC photoanode, suggesting a decisive contribution of the applied external voltage to the PEC degradation of phenol.

Significant improvement of phenol degradation with PEC process as compared to photocatalysis is shown in Figure 8b. Under UV illumination, electrons and holes were photogenerated on TiO<sub>2</sub>, enhancing charge transfer between phenyl ring and photoanodes [39] and promoting phenol degradation. However, fast recombination of these electron-hole pairs causes a low limit of phenol removal, as seen in the TiO<sub>2</sub>/UV and TiO<sub>2</sub>-AC/UV curves. The recombination time of electron-hole pairs can be longer than charge transfer time in the redox reaction under appropriate *V*<sub>app</sub>. As expected, at *V*<sub>app</sub> = 0.7 V, TiO<sub>2</sub>/PEC and TiO<sub>2</sub>-AC/PEC curves in Figure 8b exhibit an increase in phenol removal. Moreover, the TiO<sub>2</sub>-AC photoanode presents a higher efficiency of PEC degradation of phenol than the TiO<sub>2</sub> photoanode owing to the contribution of electric conductivity of AC. After 60 min of contact time, phenol PEC degradation achieved 75.9% on TiO<sub>2</sub>-AC, which is lower than that on TiO<sub>2</sub> nanotubes [40], but significantly higher than on TiO<sub>2</sub> [18].

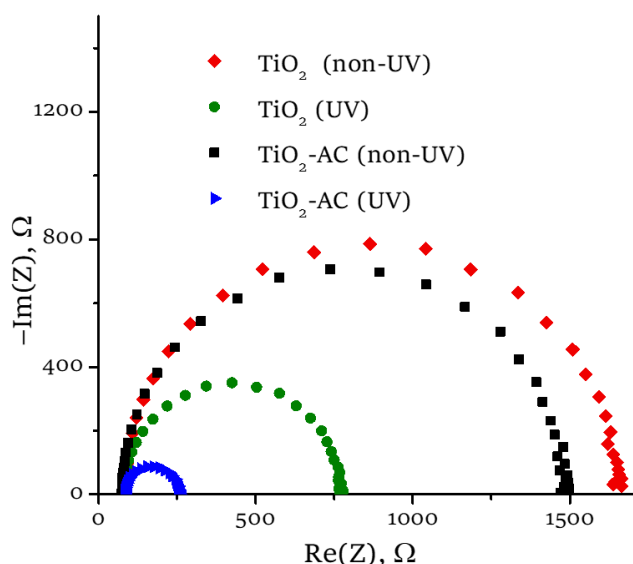


Figure 7 Nyquist plots from electrochemical impedance measurements on photoanodes in 10 mg/L of phenol solution (pH = 5).

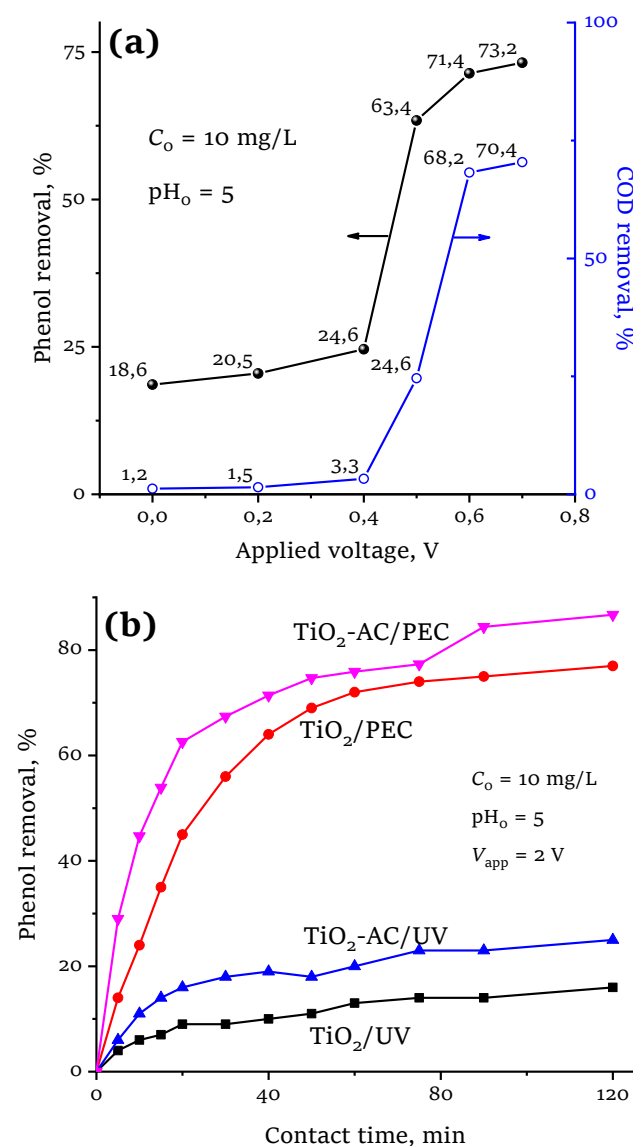


Figure 8 Effects of a) applied external voltage and b) PEC degradation of phenol on TiO<sub>2</sub>-AC photoanode.

As discussed above, the following experiments for the kinetic study of phenol PEC degradation were conducted at the TiO<sub>2</sub>-AC photoanode under  $V_{app} = 0.7$  V and UV illumination.

### 4. Kinetic of photoelectrochemical degradation of phenol in acidic solution

Photocatalytic degradation of phenol can be described by the following Langmuir - Hinshelwood (L-H) kinetic mechanism [41-42], in which phenol is first adsorbed onto the photocatalyst surface and then decomposed. Therefore, this L-H model (2) was used to fit our experimental data, revealing negative values of  $K_B$  (as shown in Table 1). However, this is unreasonable because the adsorption equilibrium constant  $K_B$  must be positive.

- L-H model: 
$$r = -\frac{dC}{dt} = \frac{K_A C}{1 + K_B C} \quad (2)$$

- First-order model: 
$$r = -\frac{dC}{dt} = k_1 C \quad (3)$$

In the case of chemical reaction control, a first-order kinetic model (3) well described the photodegradation of phenol on TiO<sub>2</sub>/AC [43] as well as ZnO, TiO<sub>2</sub> and ZnO-TiO<sub>2</sub> photocatalysts [44]. Photoelectrochemical degradation rate following the first-order model was identified for acidic red 17 dye on ammonium persulphate [45], and phenol on PbO<sub>2</sub> anode [46]. However, the determination coefficients ( $R^2$ ) obtained from fitting our experimental data with this model were not close to 1 (as shown in Table 1). It signifies that the PEC degradation of phenol occurred in a complex mechanism and was not controlled exclusively by a chemical reaction process.

We proposed a mechanism of PEC degradation of phenol through reactions (4)-(6) based on the previous reports. Spallart et al. [47] proved that water competed with aromatic compounds in PEC oxidation. Moreover, oxygen atoms from water molecules can form  $O_2^{\cdot-}$  radicals at photoexcited points [39]. Hence, the active site on the photoanode surface ( $*^{n+}$ ) was suggested to interact with a water molecule under the applied external potential and form an active site bearing oxygen ( $*^{n+} O_2^{\cdot-}$ ) following reaction (4). In other consideration, phenol (Ph) can be protonated into  $H^+Ph$  form [48] in acid solution, promoting the transfer of electron pair of oxygen in -OH group into the aromatic ring [49] and resulting in polar structure  $H^+Ph^{\delta-}$  according to reaction (5). We suppose that  $H^+Ph^{\delta-}$  contacted with  $*^{n+} O_2^{\cdot-}$  and then oxidized according to reaction (6), yielding the decomposition products and regenerating the active site.

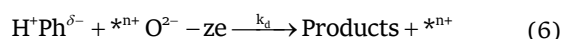
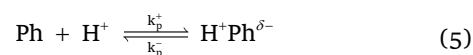
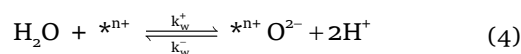


**Table 1** Calculated parameters of kinetic models at different initial concentrations and pH values.

Kinetic model	Parameters	Initial concentrations, mg/L (pH = 5)				pH values (C <sub>0</sub> = 20 mg/L)		
		5	10	15	20	3	4	6
L-H	K <sub>A</sub>	0.011	0.012	0.014	0.016	0.033	0.026	0.003
	K <sub>B</sub>	-18.62	-9.22	-5.05	-2.78	-3.073	-3.143	-4.595
	R <sup>2</sup>	0.944	0.978	0.995	0.994	0.984	0.998	0.986
First-order	k <sub>1</sub>	0.021	0.021	0.022	0.022	0.034	0.031	0.009
	R <sup>2</sup>	0.054	0.610	0.884	0.959	0.832	0.901	0.704
This study	k <sub>w</sub> <sup>+</sup>	0.131	0.070	0.204	0.122	0.013	0.241	0.231
	k <sub>w</sub> <sup>-</sup> · 10 <sup>3</sup>	5.608	5.321	6.463	6.339	5.792	6.279	6.325
	k <sub>p</sub> <sup>+</sup>	0.099	0.071	0.045	0.034	0.070	0.061	0.023
	k <sub>p</sub> <sup>-</sup>	0.032	0.024	0.022	0.013	0.009	0.027	0.028
	k <sub>d</sub> · 10 <sup>3</sup>	0.164	0.158	0.156	0.142	0.168	0.192	0.152
	[* <sup>n+</sup> ] <sub>ex</sub>	452	435	438	392	464	589	471
	R <sup>2</sup>	0.999	0.998	0.994	0.994	0.994	0.998	0.990

k<sub>1</sub> [min<sup>-1</sup>]; K<sub>A</sub> [min<sup>-1</sup>]; K<sub>B</sub> [L·mmol<sup>-1</sup>]; k<sub>w</sub><sup>+</sup>, k<sub>w</sub><sup>-</sup>, k<sub>p</sub><sup>+</sup>, k<sub>p</sub><sup>-</sup> [min<sup>-1</sup>]; k<sub>d</sub> [L·mmol<sup>-1</sup>·min<sup>-1</sup>], [\*<sup>n+</sup>]<sub>ex</sub> in mmol·L<sup>-1</sup>

We assume that reactions (4)–(6) occurred in the presence of large amounts of H<sup>+</sup> ions and H<sub>2</sub>O. Therefore, the rates of these reactions depend on the concentration of phenol (x<sub>1</sub>), H<sup>+</sup>Ph<sup>δ-</sup> (x<sub>2</sub>), and \*<sup>n+</sup>O<sup>2-</sup> (x<sub>3</sub>), as shown in equations (7), (8), (9).

$$\frac{dx_1}{dt} = -k_p^+ x_1 + k_p^- x_2, \tag{7}$$

$$\frac{dx_2}{dt} = k_p^+ x_1 - k_p^- x_2 - k_d x_2 x_3, \tag{8}$$

$$\frac{dx_3}{dt} = k_w^+ [*^{n+}] - k_w^- x_3 - k_d x_2 x_3, \tag{9}$$

where x<sub>1</sub>, x<sub>2</sub>, x<sub>3</sub> are in mmol·L<sup>-1</sup>, and [\*<sup>n+</sup>] is an apparent concentration of active sites in mmol·L<sup>-1</sup>.

Under UV illumination, TiO<sub>2</sub>-AC particles on the photoanode surface were excited to create photoexcited sites (\*). Then, under the applied external potential, the photoexcited site lost n electrons and became an active site (\*<sup>n+</sup>). Supposing that the total number of \*<sup>n+</sup> does not change with an apparent concentration [\*<sup>n+</sup>]<sub>ex</sub>, equation (10) is obtained:

$$[*^{n+}]_{ex} = x_3 + [*^{n+}]. \tag{10}$$

The value of [\*<sup>n+</sup>] can be determined from (10) and substituted in to (9) to result in (11):

$$\frac{dx_3}{dt} = k_w^+ [*^{n+}]_{ex} - (k_w^+ + k_w^- + k_d x_2) x_3. \tag{11}$$

The parameters in the proposed model (k<sub>w</sub><sup>+</sup>, k<sub>w</sub><sup>-</sup>, k<sub>p</sub><sup>+</sup>, k<sub>p</sub><sup>-</sup>, k<sub>d</sub>, and [\*<sup>n+</sup>]<sub>ex</sub>) were determined by fitting experimental data with the model using the least-square method for x<sub>1</sub> objective:

$$\sum_{i=1}^n (x_{1,i} - \widehat{x}_{1,i})^2 \rightarrow \min \tag{12}$$

where,  $\widehat{x}_1$  is the phenol concentration predicted by the model, i = 1, 2, ..., n denotes i<sup>th</sup> value, and n = 12 is the number of experimental data points.

The determination coefficient (R<sup>2</sup>) is used to evaluate the goodness of fit of the model as presented in formula (13).

$$R^2 = 1 - \frac{SSR}{SST} = 1 - \frac{(x_1 - \widehat{x}_1)^2}{(x_1 - \bar{x}_1)^2} \tag{13}$$

where SSS =  $\sum(x_1 - \widehat{x}_1)^2$  is the residual sum of squares, TSS =  $\sum(x_1 - \bar{x}_1)^2$  is the total sum of squares,  $\bar{x}_1 = \frac{1}{n} \sum_{i=1}^n x_1$  is the mean value of x<sub>1</sub>.

Numerical solutions of ordinary differential equations (7), (8), and (11) were carried out using Runge - Kutta 4<sup>th</sup> order method with initial conditions: x<sub>1</sub>(0) = [Ph]<sub>0</sub> =  $\frac{C_0}{94.11}$ , x<sub>2</sub>(0) = x<sub>3</sub>(0) = 0 (94.11 is molecule weight of phenol). The minimization problem (12) was solved with the help of the Excel Solver tool (ver. 2016) with a GRG non-linear option.

Figure 9 shows the effects of initial phenol concentration (C<sub>0</sub>) and initial pH (pH<sub>0</sub>) on phenol removal under both observations of the experiment and simulation. The proposed model exhibited a good description of the experimental data due to the closeness of R<sup>2</sup> to 1, obtaining kinetic parameters as summarized in Table 1.

Experiments of PEC degradation of phenol were performed at different C<sub>0</sub> from 5 to 20 mg·L<sup>-1</sup> at pH<sub>0</sub> = 5, revealing kinetic behavior as presented in Figure 9a. Phenol exhibits a property of UV light interception [39, 50], causing a decrease in the active site quantity (\*<sup>n+</sup>) and oxidation rate constant (k<sub>d</sub>) while increasing C<sub>0</sub> as shown in Table 1. Consequently, the rate of phenol removal is lower with higher C<sub>0</sub>. Moreover, contact time for 99.95% phenol removal was predicted to be 1110, 725, 490, and 450 minutes at C<sub>0</sub> = 5, 10, 15, and 20 mg·L<sup>-1</sup>, respectively, according to the proposed model. It proves that the PEC degradation of phenol on TiO<sub>2</sub>-AC photoanode did not reach equilibrium and tended to complete phenol removal.

pH<sub>0</sub> of the solution is an important parameter in the photodegradation of phenol because of the variation of charge properties of phenol at different pH values [51]. In this study, PEC degradation of phenol was studied at various pH<sub>0</sub> values of solution (3, 4, 5, and 6) with C<sub>0</sub> = 20 mg·L<sup>-1</sup>. Phenol is protonated to H<sup>+</sup>Ph<sup>δ-</sup> in the presence of ion H<sup>+</sup> according to reaction (4). Therefore, the lower pH<sub>0</sub> value was, the more H<sup>+</sup>Ph<sup>δ-</sup> was produced, resulting in an improvement in phenol degradation (as shown in Figure 9b).

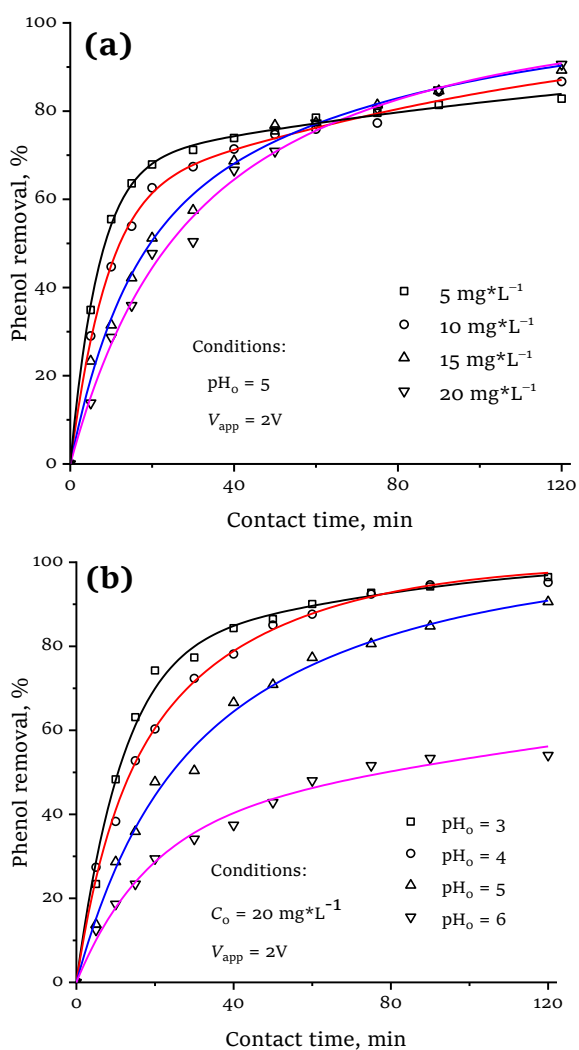


**Figure 9** Simulation (continuous line) and experimental results (discrete points) for PEC degradation kinetic of phenol on TiO<sub>2</sub>-AC photocathode at different C<sub>0</sub> (a) and pH<sub>0</sub> (b).

Variation of  $[H^+Ph^{\delta-}]/[Ph]_0$  and  $[*^{n+}O^{2-}]$  as a function of contact time at different C<sub>0</sub> was simulated and presented in Figure 10. As shown in Figure 10a,  $[H^+Ph^{\delta-}]/[Ph]_0$  increased in the first stage, then decreased, reaching the maxima around 25 minutes of contact time. A similar trend is also observed in the inset in Figure 10a, which shows the dependence of  $[H^+Ph^{\delta-}]$  on  $t$ . The higher C<sub>0</sub>, the higher maximum value of  $[H^+Ph^{\delta-}]/[Ph]_0$  would be, contrary to the  $[H^+Ph^{\delta-}]/[Ph]_0$  relation. Moreover, the rate constant  $k_p^+$  was found to be 0.099, 0.071, 0.045, and 0.034 min<sup>-1</sup> (Table 1) at 5, 10, 15, and 20 mg·L<sup>-1</sup> of C<sub>0</sub>, respectively, which proves that high C<sub>0</sub> is a disadvantage to protonation of phenol.

The curves in Figure 10b present the relationships between the amount of  $*^{n+}O^{2-}$  and the contact time. In all studied C<sub>0</sub>,  $[*^{n+}O^{2-}]$  quickly increases to reach the equilibrium concentration ( $[*^{n+}O^{2-}]_{eq}$ ). The ratios of  $[*^{n+}O^{2-}]_{eq}$  and  $[*^{n+}]_{ex}$  are larger than 0.9, as shown in the inset in Figure 10b. It means that most photoexcited sites changed to form active sites bearing oxygen, which acts as a reactant in PEC degradation of phenol. Although  $[*^{n+}O^{2-}]_{eq}$  decreased with the increase of C<sub>0</sub>, the high value (>350 mmol·L<sup>-1</sup>) was enough to interact entirely with protonated phenol molecules.

The relationship of  $[H^+Ph^{\delta-}]/[Ph]_0$  vs contact time at different pH<sub>0</sub> (3, 4, 5, and 6) exhibited maxima as shown in Figure 11a. The maximum value of  $[H^+Ph^{\delta-}]/[Ph]_0$  at pH<sub>0</sub> = 3 was the highest. At pH<sub>0</sub> = 4, 5, and 6, the maximum values of  $[H^+Ph^{\delta-}]/[Ph]_0$  were similar; however, the maximum peaks shifted to longer contact time with the increase of pH<sub>0</sub>. In other consideration from Table 1, the ratio of  $k_p^+/k_p^-$  generally decreased with the rise in pH<sub>0</sub> (7.8, 2.3, 2.6, and 0.82 at pH<sub>0</sub> = 3, 4, 5, and 6, respectively). These results prove that phenol protonation was promoted in low pH<sub>0</sub>. Moreover, pH<sub>0</sub> also affected the amount of  $*^{n+}O^{2-}$  on TiO<sub>2</sub>-AC photocathode, as shown in Figure 11b. For pH<sub>0</sub> = 4, 5, and 6,  $[*^{n+}O^{2-}]$  tended to reach  $[*^{n+}O^{2-}]_{eq}$  after around 30 minutes of contact time; and  $[*^{n+}O^{2-}]_{eq}$  at pH<sub>0</sub> = 4 was the highest. Because the point of zero charge of the prepared TiO<sub>2</sub>-AC was determined at pH = 5.4, TiO<sub>2</sub>-AC was positively charged under acidic conditions, advancing to generate  $*^{n+}O^{2-}$ . However, the amount of H<sup>+</sup> ion was too high at pH<sub>0</sub> = 3, causing a strong electrostatic force between H<sup>+</sup> and oxygen in  $*^{n+}O^{2-}$ , which dissociated oxygen and active site. Consequently,  $[*^{n+}O^{2-}]$  cannot reach equilibrium concentration after 120 minutes of contact time at pH<sub>0</sub> = 3, as shown in Figure 11b.

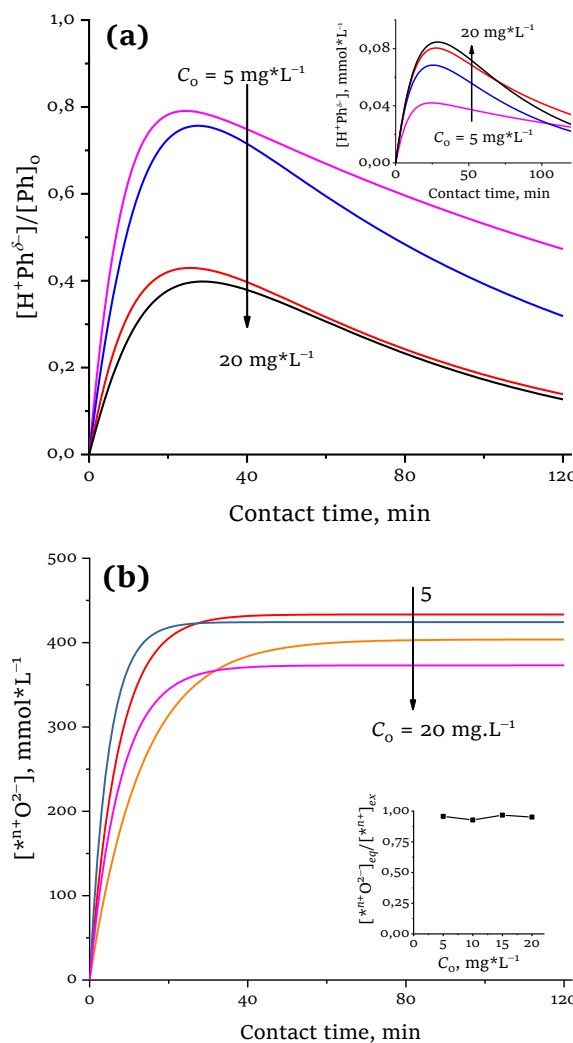


**Figure 10** Simulation of  $H^+Ph^{\delta-}$  (a) and  $*^{n+}O^{2-}$  (b) variations in PEC degradation of phenol on TiO<sub>2</sub>-AC photoanode at different C<sub>0</sub> (pH<sub>0</sub> = 5, V<sub>app</sub> = 0.7 V).

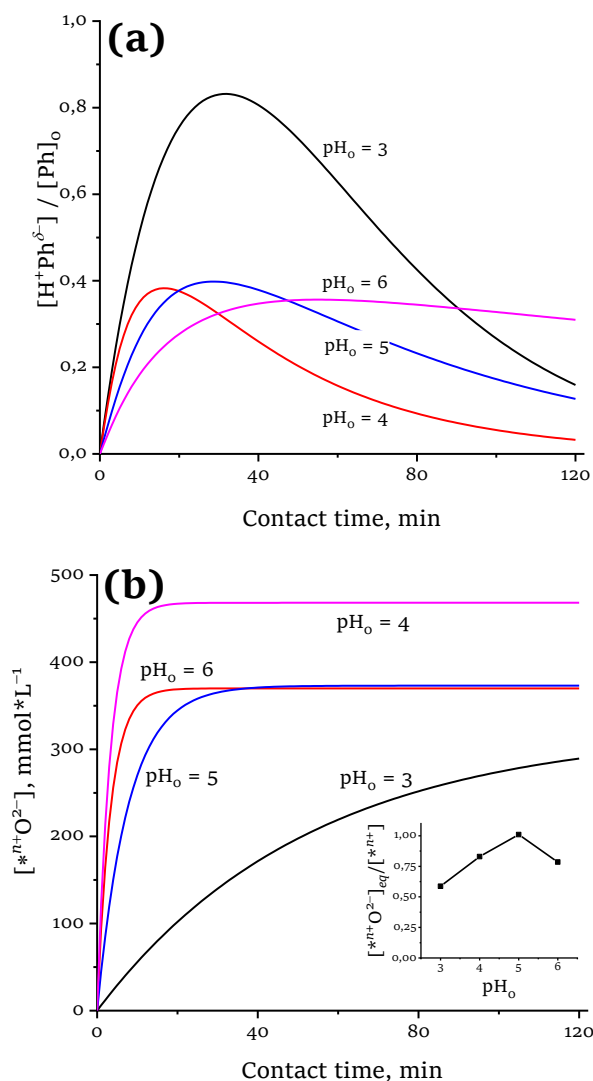


**Figure 11** Simulation of a)  $H^+Ph^{\delta-}$  and b)  $[*^{n+}O^{2-}]$  variations in PEC degradation of phenol on  $TiO_2$ -AC photoanode at different  $pH_0$  ( $C_0 = 20 \text{ mg} \cdot L^{-1}$ ,  $V_{app} = 0.7 \text{ V}$ ).

The inset in Figure 11b presents the effect of  $pH_0$  on the ratio of  $[*^{n+}O^{2-}] / [*^{n+}]_{ex}$ . It can be seen that this ratio at  $pH_0 = 5$  is the highest (close to 1). It means that more separation between the point of zero charge and  $pH_0$  caused lower  $[*^{n+}O^{2-}] / [*^{n+}]_{ex}$ .

## 5. Conclusions

In this work,  $TiO_2$  and  $TiO_2$ -AC photocatalysts were successfully synthesized by the sol-gel method to apply to the PEC degradation of phenol. The  $TiO_2$ -AC photoanode exhibits higher photoactivity for degrading phenol under UV-C illumination than  $TiO_2$ . Effects of applied external voltage, pH, and initial concentration of phenol on the kinetics of phenol PEC degradation were also experimentally investigated in this study. The interaction mechanism between protonated phenol and the active site bearing oxygen was well-demonstrated for the phenol PEC degradation. The kinetic constants and the concentration variations of protonated phenol and the active site bearing oxygen were determined by fitting the established kinetic model to the experimental data.

## Supplementary materials

No supplementary materials are available.

## Funding

This research had no external funding.

## Acknowledgments

This work was supported by the Vietnam's Ministry of Natural Resources and Environment through project coded CS.2022.12.

## Author contributions

Conceptualization: L.H.Q.A, T.D.H  
 Formal Analysis: P.V.G.N, H.T.L  
 Investigation: P.V.G.N, H.T.L  
 Methodology: L.H.Q.A., N.T.B.K, T.D.H  
 Validation: L.H.Q.A, U.P.N.T, N.T.B.K  
 Visualization: T.D.H  
 Writing – original draft: L.H.Q.A, T.D.H  
 Writing – review & editing: N.T.B.K, U.P.N.T

## Conflict of interest

The authors declare no conflict of interest.

## Additional information

Author ID:

Uyen P. N. Tran, Scopus ID [57193667111](https://orcid.org/0000-0001-9142-1000).

Websites:

Ho Chi Minh city University of Natural Resources and Environment, <https://www.hcmunre.edu.vn/>;  
 Van Hien University, <https://en.vhu.edu.vn/>;  
 Ton Duc Thang University, <https://www.tdtu.edu.vn/en>.

## References

- Albuquerque BR, Heleno SA, et al. Phenolic compounds: current industrial applications, limitations and future challenges. *Food Funct.* 2021;12(1):14–29. doi:[10.1039/DOF002324H](https://doi.org/10.1039/DOF002324H)
- Xu N, Qiu C, et al. Analysis of phenol biodegradation in antibiotic and heavy metal resistant *Acinetobacter lwoffii* NL1. *Front. Microbiol.* 2021;12:725755. doi:[10.3389/fmicb.2021.725755](https://doi.org/10.3389/fmicb.2021.725755)
- Pardeshi SK, Patil AB. A simple route for photocatalytic degradation of phenol in aqueous zinc oxide suspension using solar energy. *Sol Energy.* 2008;82(8):700–705. doi:[10.1016/j.solener.2008.02.007](https://doi.org/10.1016/j.solener.2008.02.007)
- Gupta S, Ashrith G, et al. Acute phenol poisoning: A life-threatening hazard of chronic pain relief. *Clin. Toxicol.* 2008;46(3):250–253. doi:[10.1080/15563650701438888](https://doi.org/10.1080/15563650701438888)
- Kim HY, Kim OH, Sung MK. Effects of phenol-depleted and phenol-rich diets on blood markers of oxidative stress, and urinary excretion of quercetin and kaempferol in healthy volunteers. *J Am Coll Nutr.* 2003;22(3):217–223. doi:[10.1080/07315724.2003.10719296](https://doi.org/10.1080/07315724.2003.10719296).

6. Villegas LGC, Mashhadi N, et al. A short review of techniques for phenol removal from wastewater. *Curr Pollution Rep.* 2016;2:157–167. doi:[10.1007/s40726-016-0035-3](https://doi.org/10.1007/s40726-016-0035-3)
7. Li H, Yao Y, et al. Degradation of phenol by photocatalysis using TiO<sub>2</sub>/montmorillonite composites under UV light. *Environ Sci Pollut Res.* 2022. doi:[10.1007/s11356-022-20638-8](https://doi.org/10.1007/s11356-022-20638-8)
8. Iervolino G, Zammit I, et al. Limitations and prospects for wastewater treatment by UV and visible-light-active heterogeneous photocatalysis: A critical review. *Top Curr Chem (Z).* 2020;378:7. doi:[10.1007/s41061-019-0272-1](https://doi.org/10.1007/s41061-019-0272-1)
9. Li C, Wang WD. Photocatalytic degradation of phenol over MWCNTs-TiO<sub>2</sub> composite catalysts with different diameters. *Chin J Chem Phys.* 2009;22(4):423–428. doi:[10.1088/1674-0068/22/04/423-428](https://doi.org/10.1088/1674-0068/22/04/423-428)
10. Velasco LF, Parra JB, Ania CO. Role of activated carbon features on the photocatalytic degradation of phenol. *Appl Surf Sci.* 2010;256(17):5254–5258. doi:[10.1016/j.apsusc.2009.12.113](https://doi.org/10.1016/j.apsusc.2009.12.113)
11. Malekshoar G, Pal K, et al. Enhanced solar photocatalytic degradation of phenol with coupled graphene-based titanium dioxide and zinc oxide. *Ind Eng Chem Res.* 2014;53(49):18824–18832. doi:[10.1021/ie501673v](https://doi.org/10.1021/ie501673v)
12. Yao S, Li J, Shi Z. Immobilization of TiO<sub>2</sub> nanoparticles on activated carbon fiber and its photodegradation performance for organic pollutants. *Particuol.* 2010;8(3):272–278. doi:[10.1016/j.partic.2010.03.013](https://doi.org/10.1016/j.partic.2010.03.013)
13. Nkwachukwu OV, Muzenda C, et al. Photoelectrochemical degradation of organic pollutants on a La<sup>3+</sup> doped BiFeO<sub>3</sub> perovskite. *Catalysts.* 2021;11(9):1069. doi:[10.3390/catal11091069](https://doi.org/10.3390/catal11091069)
14. Mukherjee A, Chakrabarty S, et al. Visible-light-mediated electrocatalytic activity in reduced graphene oxide-supported bismuth ferrite. *ACS Omega.* 2018;3(6):5946–5957. doi:[10.1021/acsomega.8b00708](https://doi.org/10.1021/acsomega.8b00708)
15. Bard AJ. *Photoelectrochemistry.* Sci. 1980;207(4427):139–144. doi:[10.1126/science.207.4427.13](https://doi.org/10.1126/science.207.4427.13)
16. Barham JP, Köning B. *Synthetic photoelectrochemistry.* *Angew Chem Int Ed.* 2020;59:11732–11747. doi:[10.1002/anie.201913767](https://doi.org/10.1002/anie.201913767)
17. Marwat MA, Humayun M, et al. Advanced catalysts for photoelectrochemical water splitting. *ACS Appl Energy Mater.* 2021;4(11):12007–12031. doi:[10.1021/acsaem.1c02548](https://doi.org/10.1021/acsaem.1c02548)
18. Villota-Zuleta JA, Rodríguez-Acosta, et al. Experimental data on the photoelectrochemical oxidation of phenol: Analysis of pH, potential and initial concentration. *Data Brief.* 2019;24:103949. doi:[10.1016/j.dib.2019.103949](https://doi.org/10.1016/j.dib.2019.103949)
19. Liu S, Zhao X, et al. Peroxymonosulfate enhanced photoelectrocatalytic degradation of phenol activated by Co<sub>3</sub>O<sub>4</sub> loaded carbon fiber cathode. *J Catal.* 2017;355:167–175. doi:[10.1016/j.jcat.2017.09.016](https://doi.org/10.1016/j.jcat.2017.09.016)
20. Haro M, Velasco LF, Ania CO. Carbon-mediated photoinduced reactions as a key factor in the photocatalytic performance of C/TiO<sub>2</sub>. *Catal Sci Technol.* 2012;2:2264–2272. doi:[10.1039/C2CY20270K](https://doi.org/10.1039/C2CY20270K)
21. Singh P, Singh R, et al. Effect of nanoscale TiO<sub>2</sub>-activated carbon composite on *Solanum lycopersicum* (L.) and *Vigna radiata* (L.) seeds germination. *Energy Ecol Environ.* 2016;1:131–140. doi:[10.1007/s40974-016-0009-8](https://doi.org/10.1007/s40974-016-0009-8)
22. Xing B, Shi C, et al. Preparation of TiO<sub>2</sub>/activated carbon composites for photocatalytic degradation of RhB under UV light irradiation. *J Nanomater.* 2016;2016:8393648. doi:[10.1155/2016/8393648](https://doi.org/10.1155/2016/8393648)
23. Haider A, Jameel ZN, Taha SY. Synthesis and characterization of TiO<sub>2</sub> nanoparticles via sol-gel method by pulse laser ablation. In: *The 5th International scientific Conference on Nanotechnology & Advanced Materials Their Applications*; 2015 Nov 3–4; Baghdad, Iraq. p. 761–771.
24. Arabi-Katbi OI, Pratsins SE, et al. Monitoring the flame synthesis of TiO<sub>2</sub> particles by *in-situ* FTIR spectroscopy and thermophoretic sampling. *Combust Flame.* 2001;124(4):560–572. doi:[10.1016/S0010-2180\(00\)00227-3](https://doi.org/10.1016/S0010-2180(00)00227-3)
25. Hanaor DAH, Sorrell CC. Review of the anatase to rutile phase transformation. *J Mater Sci.* 2011;46:855–874. doi:[10.1007/s10853-010-5113-0](https://doi.org/10.1007/s10853-010-5113-0)
26. Kusiak-Nejman E, Wanag A, et al. Modification of titanium dioxide with graphitic carbon from anthracene thermal decomposition as a promising method for visible-active photocatalysts preparation. *J Adv Oxid Technol.* 2016;19(2):227–235. doi:[10.1515/jaots-2016-0206](https://doi.org/10.1515/jaots-2016-0206)
27. Luttrell T, Halegamage S, et al. Why is anatase a better photocatalyst than rutile? – Model studies on epitaxial TiO<sub>2</sub> films. *Sci Rep.* 2014;4:4043. doi:[10.1038/srep04043](https://doi.org/10.1038/srep04043)
28. Liu Z, Jian Z, et al. Low-temperature reverse microemulsion synthesis, characterization, and photocatalytic performance of nanocrystalline titanium dioxide. *Int J Photoenergy.* 2012;2012:702503. doi:[10.1155/2012/702503](https://doi.org/10.1155/2012/702503)
29. Zhang H, Wang X, et al. Synthesis and characterization of TiO<sub>2</sub>/graphene oxide nanocomposites for photoreduction of heavy metal ions in reverse osmosis concentrate. *RSC Adv.* 2018;8:34241–34251. doi:[10.1039/C8RA06681G](https://doi.org/10.1039/C8RA06681G)
30. Muhammad AS, Naser JT, et al. Photocatalytic degradation of methylene blue and phenol using TiO<sub>2</sub>/activated-carbon composite catalysts. *Asian J Chem.* 2015;27(1): 343–348. doi:[10.14233/ajchem.2015.17936](https://doi.org/10.14233/ajchem.2015.17936)
31. Greco G, Mazzio KA, et al. Structural study of carbon-coated TiO<sub>2</sub> anatase nanoparticles as high-performance anode materials for Na-Ion batteries. *ACS Appl Energy Mater.* 2019;2(10):7142–7151. doi:[10.1021/acsaem.9b01101](https://doi.org/10.1021/acsaem.9b01101)
32. Wang H, Xia Y, et al. Highly active deficient ternary sulfide photoanode for photoelectrochemical water splitting. *Nat Commun.* 2020;11:3078. doi:[10.1038/s41467-020-16800-w](https://doi.org/10.1038/s41467-020-16800-w)
33. Doménech-Carbó A, Doménech-Carbó MT, Costa V. *Electrochemical Methods in Archaeometry, Conservation and Restoration.* Springer-Verlag Berlin Heidelberg: New York; 2009. 199 p.
34. Jung H, Chae SY, et al. Effect of the Si/TiO<sub>2</sub>/BiVO<sub>4</sub> heterojunction on the onset potential of photocurrents for solar water oxidation. *ACS Appl Mater Interfaces.* 2015;7(10):5788–5796. doi:[10.1021/am5086484](https://doi.org/10.1021/am5086484)
35. Bertolizzi L, Bisquert J. Equivalent circuit of electrons and holes in thin semiconductor films for photoelectrochemical water splitting applications. *J Phys Chem Lett.* 2012;3(17):2517–2522. doi:[10.1021/jz301090g](https://doi.org/10.1021/jz301090g)
36. Qu J, Li GR, Gao XP. One-dimensional hierarchical titania for fast reaction kinetics of photoanode materials of dye-sensitized solar cells. *Energy Environ Sci.* 2010;3:2003–2009. doi:[10.1039/C003646C](https://doi.org/10.1039/C003646C)
37. Sun Y, Yan KP. Effect of anodization voltage on performance of TiO<sub>2</sub> nanotube arrays for hydrogen generation in a two-compartment photoelectrochemical cell. *Int J Hydrog Energy.* 2014;22:11368–11375. doi:[10.1016/j.ijhydene.2014.05.115](https://doi.org/10.1016/j.ijhydene.2014.05.115)
38. Grabowska E, Reszczyńska J, Zaleska. Mechanism of phenol photodegradation in the presence of pure and modified-TiO<sub>2</sub>: A review. *Water Res.* 2012;46(17):5453–5471. doi:[10.1016/j.watres.2012.07.048](https://doi.org/10.1016/j.watres.2012.07.048)
39. Mohamed A, Yousef S, et al. Rapid photocatalytic degradation of phenol from water using composite nanofibers under UV. *Environ Sci Eur.* 2020;32:160. doi:[10.1186/s12302-020-00436-0](https://doi.org/10.1186/s12302-020-00436-0)
40. Orudzhev<sup>z</sup> FF, Aliev ZM, et al. Photoelectrocatalytic oxidation of phenol on TiO<sub>2</sub> nanotubes under oxygen pressure. *Russ J Electrochem.* 2015;51(12):1108–1114. doi:[10.1134/S1023193515110130](https://doi.org/10.1134/S1023193515110130)
41. Asenjo NG, Santamaría, et al. Correct use of the Langmuir-Hinshelwood equation for proving the absence of a synergy effect in the photocatalytic degradation of phenol on a suspended mixture of titania and activated carbon. *Carbon.* 2013;55:62–69. doi:[10.1016/j.carbon.2012.12.010](https://doi.org/10.1016/j.carbon.2012.12.010)
42. Zamri MSFA, Sapwe N. Kinetic study on photocatalytic degradation of phenol using green electrosynthesized TiO<sub>2</sub> nanoparticles. *Materialstoday: Proceedings.* 2019;19(4):1261–1266. doi:[10.1016/j.matpr.2019.11.131](https://doi.org/10.1016/j.matpr.2019.11.131)

43. Alalm MG, Tawfik A, Ookawara S. Solar photocatalytic degradation of phenol by TiO<sub>2</sub>/AC prepared by temperature impregnation method. *Desalination Water Treat.* 2016;57(2):835–844. doi:[10.1080/19443994.2014.969319](https://doi.org/10.1080/19443994.2014.969319)
44. Prabha I, Lathasree S. Photodegradation of phenol by zinc oxide, titania and zinc oxide–titania composites: Nanoparticle synthesis, characterization and comparative photocatalytic efficiencies. *Mater Sci Semicond Process.* 2014;26:603–613. doi:[10.1016/j.mssp.2014.05.031](https://doi.org/10.1016/j.mssp.2014.05.031)
45. Thabet M, El-Zomrawy AA. Degradation of acid red 17 dye with ammonium persulphate in acidic solution using photoelectrocatalytic methods. *Arab J Chem.* 2016;9:S204–S208. doi:[10.1016/j.arabjc.2011.03.001](https://doi.org/10.1016/j.arabjc.2011.03.001)
46. Duan X, Ma F, et al. Electrochemical degradation of phenol in aqueous solution using PbO<sub>2</sub> anode. *J Taiwan Inst Chem Eng.* 2013;44:95–102. doi:[10.1016/j.jtice.2012.08.009](https://doi.org/10.1016/j.jtice.2012.08.009)
47. Neumann-Spallart M, Shinde SS, et al. Photoelectrochemical degradation of selected aromatic molecules. *Electrochim Acta.* 2013;111:830–836. doi:[10.1016/j.electacta.2013.08.080](https://doi.org/10.1016/j.electacta.2013.08.080)
48. Katada M, Fujii A. Infrared spectroscopy of protonated phenol–water clusters. *J Phys Chem A.* 2018;122(27):5822–5831. doi:[10.1021/acs.jpca.8b04446](https://doi.org/10.1021/acs.jpca.8b04446)
49. Granucci G, Hynes JT, et al. A theoretical investigation of excited-state acidity of phenol and cyanophenols. *J Am Chem Soc.* 2000;122(49):12243–12253. doi:[10.1021/ja993730j](https://doi.org/10.1021/ja993730j)
50. Balaska A, Samar ME, Grid A. Phenol photodegradation process assisted with Wells–Dawson heteropolyacids. *Desalination Water Treat.* 2015;54(2):382–392. doi:[10.1080/19443994.2014.883577](https://doi.org/10.1080/19443994.2014.883577)
51. Dubale AA, Ahmed IN, et al. A highly stable metal–organic framework derived phosphorus doped carbon/Cu<sub>2</sub>O structure for efficient photocatalytic phenol degradation and hydrogen production. *J Mater Chem A.* 2019;7:6062–6079. doi:[10.1039/C8TA12544A](https://doi.org/10.1039/C8TA12544A)